JAERI-Research
96-006

STUDY OF FAST WAVE CURRENT DRIVE IN A KT-2 TOKAMAK PLASMA

February 1996

Bong G. HONG* and Kiyotaka HAMAMATSU

日本原子力研究所
Japan Atomic Energy Research Institute

本レポートは，日本原子力研究所が不定期に公刊している研究報告書です。

入手の問合わせは，日本原子力研究所技術情報部情報資料課（〒319-11 茨城県那珂郡東海村）あて，お申し越しください。なお，このほかに財団法人原子力弘済会資料センター（〒319-11 茨城県那珂郡東海村日本原子力研究所内）で複写による実費頒布をおこなっております。

This report is issued irregularly.

Inquiries about availability of the reports should be addressed to Information Division, Department of Technical Information, Japan Atomic Energy Research Institute, Tokai-mura, Naka-gun, Ibaraki-ken 319-11, Japan.

編集兼発行　日本原子力研究所

印　　刷　㈱原子力資料サービス

Study of Fast Wave Current Drive in a KT－2 Tokamak Plasma

Bong G. HONG* and Kiyotaka HAMAMATSU

Department of Fusion Plasma Research
Naka Fusion Research Establishment
Japan Atomic Energy Research Institute
Naka-machi, Naka-gun, Ibaraki-ken

(Received January 16, 1996)

Global analysis of fast wave current drive in a KT－2 tokamak plasma is performed by using the code, TASKW1, developed by JAERI and Okayama University (Dr. Fukuyama) , which solves the kinetic wave equation in a one dimensional slab geometry. A phase-shifted antenna array is used to inject toroidal momentum to electrons. To find guidelines of optimum antenna design for efficient current drive, accessibility conditions are derived. The dependence of the current drive efficiency on launching conditions such as the total number of antennas, phase and spacing is investigated for two cases of wave frequency; $f = 30$ MHz ($< f_{cH}$) and $f = 225$ MHz ($= 5 f_{cH}$) .

Keywords: Fast Wave, Current Drive, KT-2, Tokamak, Kinetic, Wave Equation, Antenna Array

* Visiting scientist from Korea Atomic Energy Research Institute under the Scientist Exchange Program of Science and Technology Agency of Japan.

KT－2トカマク・プラズマにおける速波電流駆動の解析

日本原子力研究所那珂研究所炉心プラズマ研究部
洪　　鳳根*・浜松　清隆

（1996年1月16日受理）

KT－2トカマク・プラズマにおける速波電流駆動の数値解析を行なった。数値解析は運動論的波動伝播方程式を1次元スラブ配位で大域的に解析するTASKW1コードを用いて行なった。尚，このコードは原研と岡山大学（福山博士）の協力研究の下で開発・改良された。電流位相制御されたアンテナ列によってトロイダル方向への運動量が電子へ入射される。この時，電流駆動を効率良く行なう為の最適なアンテナ設計の指針を得る為，波動の近接条件の評価から行なった。2つの周波数帯，$f = 30$ MHz（$< f_{cH}$）と$f = 225$ MHz（$= 5 f_{cH}$）の速波に対して，アンテナの本数及びその間隔等の入射条件と電流駆動効率の関係を求めた。

那珂研究所：〒311－01　茨城県那珂郡那珂町向山801－1
＊科学技術庁原子力研究交流制度に基づく研究員（韓国原子力研究所）

Contents

目　　次

1 Introduction

For an economically viable steady state tokamak reactor, simultaneous achievement of high $\beta_N(\equiv \frac{\beta}{I_p/aB_0})$, high confinement enhancement, and a large, well-aligned bootstrap current fraction is necessary. Although recent experiments have achieved one or two of these conditions successfully[1-3], simultaneous achievement of all requirements, i.e. "advanced tokamak operation", has not yet been demonstrated. Operation scenarios with an inverted q profile are promising candidates for advanced tokamak mode and have been shown[4,5] to yield enhanced MHD stability and confinement in the core. To maintain plasma current and MHD stability at high β, high bootstrap current fraction plasma, current drive, and current profile control by non-inductive current drive methods are a prerequisite. Lower hybrid wave[6,7] has been used to drive current in the off-axis region due to its density cut-off. In contrast, fast wave current drive appears to be an attractive method for the seed current near magnetic axis since it can penetrate into plasma center and deposit energy and momentum. The KT-2 tokamak[8] has been conceptualized to have a large aspect ratio of 5.6 with intense RF heating, so that advanced tokamak research in case of high bootstrap current fraction is allowed. For KT-2, FWCD(Fast Wave Current Drive) was chosen as a main drive for the seed current at the center.

Among many issues associated with FWCD, the most important one for KT-2 is thought to be the design of an antenna system with efficient current drive, i.e. to keep the given RF energy and momentum from going to ions or other loss channels. This requires the investigation of the fast wave spectra for various wave frequencies, plasma parameters and launching conditions, such as antenna phasing, spacing and the total number of antennas. To solve FWCD problems, several theoretical and numerical studies[9-12] have been performed. The complete plasma-antenna system was investigated quantitatively in Ref.12 and applied to a JFT-2M tokamak plasma. In this study, we apply the analyses of ICRF wave propagation[13,14] to obtain induced current. The kinetic treatment of the dispersion relation enables the inclusion of various kinetic effects such as mode conversion to the ion Bernstein wave, electron Landau damping, and ion cyclotron damping. Also, by solving the wave equation as a boundary value problem, the tunneling effect, standing wave formation, and antenna coupling can be described, which the ray tracing analysis[15] cannot describe. For a KT-2 plasma, application of the ray tracing method is dif-

ficult since the wavelength of the ICRF wave is comparable to the scale lengths of the equilibrium densities and temperatures.

In Section 2 we describe the basic model equations. The accessibility conditions and optimum antenna parameters are given in Section 3. The phase dependence on antenna launching conditions are investigated in Section 4 for two wave frequencies; $f = 30\,MHz$ and $f = 225\,MHz$. Finally we summarize our findings for the optimum antenna design in Section 5.

2 Plasma Model and Wave Equations

In this section, we describe a one-dimensional model of ICRF wave propagation. As shown in Fig. 1, the magnetic field is in the z-direction and the magnitude varies in the x-direction as

$$B(x) = \frac{B_0}{1 + x/R}, \tag{1}$$

simulating a toroidal system. The surfaces of plasma are at $x = \pm a$, and the plasma is assumed to be homogeneous in the y and z direction. The plasma density and temperature profiles are assumed to be parabolic given by

$$n_s(x) = (n_{s0} - n_b)(1 - \frac{x^2}{a^2}) + n_b \tag{2}$$

$$T_s(x) = (T_{s0} - T_b)(1 - \frac{x^2}{a^2}) + T_b \tag{3}$$

where n_b and T_b are the density and temperature at the plasma boundaries.

The model antenna is placed at $x = d$ on the low field side and carries a sheet current in the y direction with a frequency, $\omega(= 2\pi f)$. Then the z profile of the antenna current density, $J_y^A(z)$ is Fourier-decomposed as

$$J_y^A(z) = \sum_{k_z} J^A(k_z)\delta(x - d)exp(ik_z z - i\omega t) \tag{4}$$

The wave fields in the plasma are described by Maxwell's equations ;

$$\nabla \times \mathbf{E} = i\omega\mathbf{B} \tag{5}$$

and

$$\nabla \times \mathbf{B} = -i\frac{\omega}{c^2}\mathbf{E} + \mu_0(\sum_s \mathbf{J}_s + \mathbf{J}^A) \tag{6}$$

where s denotes the particle species and $\mathbf{J}_s$ is the oscillating current carried by the s-th species which is calculated from the nonlocal kinetic dielectric tensor[13] ;

ficult since the wavelength of the ICRF wave is comparable to the scale lengths of the equilibrium densities and temperatures.

In Section 2 we describe the basic model equations. The accessibility conditions and optimum antenna parameters are given in Section 3. The phase dependence on antenna launching conditions are investigated in Section 4 for two wave frequencies; $f = 30\,MHz$ and $f = 225\,MHz$. Finally we summarize our findings for the optimum antenna design in Section 5.

2 Plasma Model and Wave Equations

In this section, we describe a one-dimensional model of ICRF wave propagation. As shown in Fig. 1, the magnetic field is in the z-direction and the magnitude varies in the x-direction as

$$B(x) = \frac{B_0}{1 + x/R}, \tag{1}$$

simulating a toroidal system. The surfaces of plasma are at $x = \pm a$, and the plasma is assumed to be homogeneous in the y and z direction. The plasma density and temperature profiles are assumed to be parabolic given by

$$n_s(x) = (n_{s0} - n_b)(1 - \frac{x^2}{a^2}) + n_b \tag{2}$$

$$T_s(x) = (T_{s0} - T_b)(1 - \frac{x^2}{a^2}) + T_b \tag{3}$$

where n_b and T_b are the density and temperature at the plasma boundaries.

The model antenna is placed at $x = d$ on the low field side and carries a sheet current in the y direction with a frequency, $\omega(= 2\pi f)$. Then the z profile of the antenna current density, $J_y^A(z)$ is Fourier-decomposed as

$$J_y^A(z) = \sum_{k_z} J^A(k_z)\delta(x - d)exp(ik_z z - i\omega t) \tag{4}$$

The wave fields in the plasma are described by Maxwell's equations ;

$$\nabla \times \mathbf{E} = i\omega\mathbf{B} \tag{5}$$

and

$$\nabla \times \mathbf{B} = -i\frac{\omega}{c^2}\mathbf{E} + \mu_0(\sum_s \mathbf{J}_s + \mathbf{J}^A) \tag{6}$$

where s denotes the particle species and $\mathbf{J}_s$ is the oscillating current carried by the s-th species which is calculated from the nonlocal kinetic dielectric tensor[13] ;

$$\mathbf{J}_s(r) = \int \sigma[r - r', (r + r')/2]\mathbf{E}(r')dr' \tag{7}$$

The explicit form of $\mathbf{J}_s$ was calculated using the kinetic treatment in Ref.13. In calculating the conductivity tensor σ_s, the inhomogeneity of the equilibrium was assumed to be weak compared with the gyroradius and the second order correction from finite gyroradius effects was retained. Mode conversion to the hot branch, Landau damping, and cyclotron damping near the fundamental and second harmonics resonances are included. The electron power absorption mechanism includes Landau damping, transit time magnetic pumping, and the cross term between E_y and E_z.

Eqs.(5)-(7) are solved to obtain the wave field in the plasma region, which is connected to the wave field in the vacuum region. In the vacuum region, the solution is determined by the boundary conditions at $\tilde{x} = \pm b$ (on the wall) and $x = d$ (on the antenna). Across the current sheet,

$$\frac{dE_y}{dx}\Big|_{d-0}^{d+0} = -i\omega\mu_0 J_y^A \tag{8}$$

has to be satisfied due to the jump in $\frac{dE_y}{dx}$, and at walls we use the boundary condition

$$\frac{1}{E_y}\frac{dE_y}{dx}\Big|_{\pm b} = \mp\sqrt{\{k_z^2 - (1 + \frac{i\sigma_W}{\omega\epsilon_0})\frac{\omega^2}{c^2}\}}. \tag{9}$$

In Eq.(9) σ_W denotes the conductivity of the wall; therefore, RF energy is dissipated on the wall due to the finite resistivity. This loss plays an important role in determining the coupling efficiency of the antenna. At the plasma-vacuum interface, we employ a boundary condition where perfect reflection of the ion Bernstein wave is assumed.

The power absorption density per unit volume of the species s is given by

$$P_s = < \mathbf{J}_s \cdot \mathbf{E} >, \tag{10}$$

where $< \cdots >$ denotes the average over the wave period. By integrating Eq.(10) over x, we define the power input per unit length as

$$\bar{P}_s = \int_{-a}^{a} dx < \mathbf{J}_s \cdot \mathbf{E} > 2\pi R, \tag{11}$$

and the power loss to the walls as

$$\bar{P}_W = \frac{\pi R}{\mu_0\omega}\{|Im(E_y^\dagger \frac{dE_y}{dx})_{x=-b}| + |Im(E_y^\dagger \frac{dE_y}{dx})_{x=b}|\}, \tag{12}$$

where the symbol † denotes the complex conjugate. The total power input per unit antenna length is expressed as

$$\bar{P}_A = \sum_s \bar{P}_s + \bar{P}_W. \tag{13}$$

For a given antenna current $\mathbf{J}^A$, eqs. (5)-(9) are solved using a one dimensional ICRF wave code[13] in slab geometry. In this code the wave equation is solved along the direction of major radius(x direction) with periodic boundary conditions in the toroidal direction. The detailed numerical procedure for solving Eqs. (5)-(9) is given in Ref. 13.

The global current drive efficiency η_G is defined as the ratio of the total induced current to the total emitted power from the antenna ;

$$\eta_G = \frac{\bar{J}}{\bar{P}_A}, \tag{14}$$

where $\bar{J} = \int_{-a}^{a} J(x)dx$. In calculating the induced current $\bar{J}$, contributions from electron Landau damping, transit time magnetic pumping, and cross terms are taken into account. A fitting formula derived by Ehst and Karney[16] was used.

3 Antenna Design

In this section, we present numerical results on fast wave current drive in a KT-2 tokamak plasma. Typical plasma parameters of the KT-2 tokamak are shown in Table 1. In this study we consider two cases with different wave frequency; 30 *MHz* and 225 *MHz*.

3.1 Accessibility condition

A fast wave can be absorbed by electrons depending on the parallel wave number k_z. To find out the accessible region of k_z, we investigate the spectra of power absorption as a function of the parallel wave number k_z. Fig. 2 shows the power absorption and the current drive efficiency defined in Eq.(14) for $n_0 = 1 \times 10^{20}\, m^{-3}$, $T_0 = 5\ keV$, $f = 30\ MHz$, and an antenna current density of $J(k_z) = 1\ A/m$. The current drive efficiency reaches a maximum at $k_z = 3\, m^{-1}$ and decreases as k_z increases. The power absorption spectra show several sharp peaks due to cavity resonance effects[17]. Power absorption by the ions is negligible in this case. The upper limit of the accessible region is found to be $12 m^{-1}$. Investigation of the spatial

where the symbol † denotes the complex conjugate. The total power input per unit antenna length is expressed as

$$\bar{P}_A = \sum_s \bar{P}_s + \bar{P}_W. \tag{13}$$

For a given antenna current $\mathbf{J}^A$, eqs. (5)-(9) are solved using a one dimensional ICRF wave code[13] in slab geometry. In this code the wave equation is solved along the direction of major radius(x direction) with periodic boundary conditions in the toroidal direction. The detailed numerical procedure for solving Eqs. (5)-(9) is given in Ref. 13.

The global current drive efficiency η_G is defined as the ratio of the total induced current to the total emitted power from the antenna ;

$$\eta_G = \frac{\bar{J}}{\bar{P}_A}, \tag{14}$$

where $\bar{J} = \int_{-a}^{a} J(x)dx$. In calculating the induced current $\bar{J}$, contributions from electron Landau damping, transit time magnetic pumping, and cross terms are taken into account. A fitting formula derived by Ehst and Karney[16] was used.

3 Antenna Design

In this section, we present numerical results on fast wave current drive in a KT-2 tokamak plasma. Typical plasma parameters of the KT-2 tokamak are shown in Table 1. In this study we consider two cases with different wave frequency; 30 *MHz* and 225 *MHz*.

3.1 Accessibility condition

A fast wave can be absorbed by electrons depending on the parallel wave number k_z. To find out the accessible region of k_z, we investigate the spectra of power absorption as a function of the parallel wave number k_z. Fig. 2 shows the power absorption and the current drive efficiency defined in Eq.(14) for $n_0 = 1 \times 10^{20}\, m^{-3}$, $T_0 = 5\ keV$, $f = 30\ MHz$, and an antenna current density of $J(k_z) = 1\ A/m$. The current drive efficiency reaches a maximum at $k_z = 3\, m^{-1}$ and decreases as k_z increases. The power absorption spectra show several sharp peaks due to cavity resonance effects[17]. Power absorption by the ions is negligible in this case. The upper limit of the accessible region is found to be $12 m^{-1}$. Investigation of the spatial

profiles of electron power absorption induced current shows that when k_z is bigger than $12\,m^{-1}$, the fast wave is evanescent due to fast wave cut-off and surface current develops at the peripheral plasma region.

Fig. 3 shows that when the temperature increases to 10 keV with other parameters the same as Fig. 2, the lower wave number region becomes accessible but the upper limit remains unchanged. The current drive efficiency is bigger than the low temperature(5 keV) case. When the density decreases, the current drive efficiency increases compared with the higher density case(Fig. 2) as shown in Fig. 4 for the case of $n_0 = 0.5 \times 10^{20}\ m^{-3}$ and $T_0 = 5\ keV$.

In Fig. 5, we show the power absorption spectra for $n_0 = 1 \times 10^{20} m^{-3}$, $T_0 = 5 keV$ and $f = 225\ MHz$. The lower and upper limit of the accessible region increase and are found to be $k_{z,min} = 12\ m^{-1}$ and $k_{z,max} \doteq 90\ m^{-1}$, respectively. The current drive efficiency reaches a maximum around $k_z = 18\ m^{-1}$ and is bigger than low frequency case(Fig. 2). In this case power absorption by the ions is not negligible up to $k_z = 20\ m^{-1}$.

Accessibility diagrams such as Figs. 2 - 5 can be used to determine guidelines for optimum antenna design for efficient current drive.

3.2 Optimum antenna parameters

We consider multiple antennas at locations $z_j = (j-1)\Delta z$ with phase $\phi_j = (j-1)\Delta\phi$ (j runs from 1 to N, where N is the total number of antennas). The time varying antenna current is given by

$$\mathbf{J}^A = \begin{pmatrix} 0 \\ 1 \\ 0 \end{pmatrix} J^A(z)\delta(x-d)exp(-i\omega t). \tag{15}$$

The antenna current distribution, $J^A(z)$, is expressed as

$$J^A(z) = \sum_{j=1}^{N} J_j^A(z)exp(i\phi_j). \tag{16}$$

For constant antenna current densities, i.e. $J_j^A(z) = J_0$, the spectrum of the antenna current is given by

$$|J(k_z)| = 2J_0 \left| \frac{sin(k_z \Delta W/2)}{k_z} \right| \left| \frac{1 - cosN(\Delta\phi - k_z\Delta z)}{1 - cos(\Delta\phi - k_z\Delta z)} \right| \tag{17}$$

Here, ΔW represents the width of the antenna. The dominant spectrum peak and

it's width are calculated to be

$$k_{z,m} = \frac{\Delta\phi - 2\pi m}{\Delta z} \quad \text{for m=0, } \pm 1, \pm 2, \cdots \tag{18}$$

$$\Delta k_z = \frac{4\pi}{N\Delta z}. \tag{19}$$

Eq. (19) shows that as total number of antennas increases, Δk_z decreases. We will discuss the effect of this in next section.

For efficient current drive, the antenna parameters can be optimized by requiring that the current is driven mainly by the $m = 0$ spectrum peak corresponding to the optimum wave number found in Figs. 2 - 5. The $m = 1$ spectrum peak is removed from accessibility since it induces counter current and reduces the current drive efficiency. This condition gives

$$\Delta z \leq \frac{2\pi}{k_{z,max} + k_{z,m=0}}. \tag{20}$$

Also, the condition

$$k_{z,m=0} \leq k_{z,max} \tag{21}$$

restricts the change of the antenna phase for a given antenna spacing since Eq. (21) reduces to

$$\Delta\phi \leq \Delta z \cdot k_{z,max}. \tag{22}$$

For the wave frequency of $30 MHz$, we obtain $\Delta z \leq 41.9 cm$, since $k_{z,max} = 12 m^{-1}$ and $k_{z,m=0} = 3\ m^{-1}$ from Fig. 2. For the higher wave frequency of 225 MHz and for phase variation up to π, we obtain $3.5\ cm \leq \Delta z \leq 5.9\ cm$ from Fig. 5. This condition is rather restrictive and hardly realizable.

4 Dependence on Launching Conditions

In this section, we present the parametric dependence of fast wave current drive on the launching conditions. The results in this section are for the case of plasma parameters given in Table 1 and fixed total antenna radiation power, $\bar{P}_A = 1 MW/m$.

4.1 Low frequency excitation; $f = 30\ MHz$

Fig. 6 shows the phase dependence of the power absorption, induced current, average resistance($\bar{R} = \sum_{j=1}^{N} Re(Z_j)/N$) and reactance ($\bar{X} = \sum_{j=1}^{N} Im(Z_j)/N$) per antenna for the case of N=4 and $\Delta z = 12.2\ cm$, where Z_j is the loading impedance of the

it's width are calculated to be

$$k_{z,m} = \frac{\Delta\phi - 2\pi m}{\Delta z} \quad \text{for m=0, } \pm 1, \pm 2, \cdots \tag{18}$$

$$\Delta k_z = \frac{4\pi}{N\Delta z}. \tag{19}$$

Eq. (19) shows that as total number of antennas increases, Δk_z decreases. We will discuss the effect of this in next section.

For efficient current drive, the antenna parameters can be optimized by requiring that the current is driven mainly by the $m = 0$ spectrum peak corresponding to the optimum wave number found in Figs. 2 - 5. The $m = 1$ spectrum peak is removed from accessibility since it induces counter current and reduces the current drive efficiency. This condition gives

$$\Delta z \leq \frac{2\pi}{k_{z,max} + k_{z,m=0}}. \tag{20}$$

Also, the condition

$$k_{z,m=0} \leq k_{z,max} \tag{21}$$

restricts the change of the antenna phase for a given antenna spacing since Eq. (21) reduces to

$$\Delta\phi \leq \Delta z \cdot k_{z,max}. \tag{22}$$

For the wave frequency of $30\,MHz$, we obtain $\Delta z \leq 41.9cm$, since $k_{z,max} = 12m^{-1}$ and $k_{z,m=0} = 3\ m^{-1}$ from Fig. 2. For the higher wave frequency of 225 MHz and for phase variation up to π, we obtain $3.5\ cm \leq \Delta z \leq 5.9\ cm$ from Fig. 5. This condition is rather restrictive and hardly realizable.

4 Dependence on Launching Conditions

In this section, we present the parametric dependence of fast wave current drive on the launching conditions. The results in this section are for the case of plasma parameters given in Table 1 and fixed total antenna radiation power, $\bar{P}_A = 1MW/m$.

4.1 Low frequency excitation; $f = 30\ MHz$

Fig. 6 shows the phase dependence of the power absorption, induced current, average resistance($\bar{R} = \sum_{j=1}^{N} Re(Z_j)/N$) and reactance ($\bar{X} = \sum_{j=1}^{N} Im(Z_j)/N$) per antenna for the case of N=4 and $\Delta z = 12.2\ cm$, where Z_j is the loading impedance of the

j-th antenna defined by

$$Z_j = \frac{\int dz E_y(z) J_j^A(z) exp(i\phi_j)}{\int dz J_j^A(z)^2}. \tag{23}$$

According to the condition given in Eq. (22), the phase can be varied up to $\Delta\phi = 82.5°$ with the antenna spacing, $\Delta z = 12.2cm$. The power absorption by electrons is almost constant as shown in Fig. 6(a). The loading resistance increases with $\Delta\phi$ and reaches a maximum around $\Delta\phi = 70°$, while the loading reactance is almost constant(Fig. 6(b)). Fig. 6(c) shows that the current drive efficiency increases until $\Delta\phi = 20°$ and remains almost constant for $\Delta\phi > 20°$. For $\Delta\phi < 20°$, the contribution from the small k_z region($< 3\ m^{-1}$) to the current is small, but for $\Delta\phi > 20°$, the width of the dominant peak of the antenna current spectrum, Δk_z, is in the accessible regions where the efficiency is large as shown in Fig. 2. In Fig. 7, we show the antenna current spectrum for $\Delta\phi = 70°$. The power absorption spectrum is determined by the product between the absorption spectrum such as in Fig. 2 and the antenna current spectrum. In Fig. 7 the other N-2 subpeaks reduce the current drive efficiency and the ratio of the dominant peak to the subpeaks is roughly estimated as $1/N$ from Eq.(17).

For comparison we show the phase dependence of electron power absorption, loading impedance, and current drive efficiency for the case of N=8 in Fig. 8. In this case, the dominant spectrum width, Δk_z, is smaller than the $N = 4$ case and the current drive efficiency increases with $\Delta\phi$ and reaches a maximum around $\Delta\phi = 70°$. Fig. 9 shows spatial structure of energy flux and electron power absorption(a), induced current(b), and the electric fields(E_y(c), E_z(d)) for the case of $\Delta\phi = 70°$ and N=8. The decrease of energy flux shows that the spatial damping of the incident fast wave and the induced current profile follow the electron absorption profile. Electron power is absorbed in the central region and results in peaking of the induced current in the central region. Fig. 9(c) and (d) show the formation of a standing wave with radial mode number 4.

When we increase the antenna spacing, $\Delta z = 24.4cm$, the phase can be varied up to 165° as indicated by Eq. (22) and the dominant spectrum width, Δk_z, decreases. Figure 10 shows the phase dependence of the power absorption, induced current and average resistance and reactance per antenna for the case of N=4 and $\Delta z = 24.4\ cm$. As in the $\Delta z = 12.2\ cm$ case, the power absorption by electrons is almost

constant(Fig. 10(a)). The loading resistance is a maximum at $\Delta\phi = 130°$, while the loading reactance is almost constant(Fig. 10(b)). The current drive efficiency increases with $\Delta\phi$ and reaches a maximum around $\Delta\phi = 130°$. It is noted that the curve shape is similar to that of Fig. 8(c). This is because increasing the spacing and increasing the number of antennas have the same effect in reducing Δk_z except for contributions from subpeaks in the antenna current spectrum.

As shown in Fig. 11, in the case of N=8 with $\Delta z = 24.4\,cm$, several peaks in the current drive efficiency appear since different k_z values can be selectively excited due to smaller Δk_z.(Fig.11) Maximum efficiency can be obtained by selectively exciting $k_z = 9\,m^{-1}(\Delta\phi = 130°)$.

The spatial structure of the electron power absorption and induced current for the case of $\Delta\phi = 140°$ and N=8 are similar to the case shown in Fig. 9.

4.2 High frequency excitation; $f = 225\,MHz$

As found in Sec.3 the exclusion of the m=1 peak of the antenna current spectrum from the accessibility region is hard to satisfy with realizable antenna spacing. In this section, we investigate the characteristics of high frequency excitation with the antenna spacing $\Delta z = 12.2\,cm$.

Fig. 12(a) shows the phase dependence of power absorption when the total number of antennas is $N = 8$. Power absorption by ions is not negligible and is larger than absorption by the electrons for $20° < \Delta\phi < 120°$. Both the loading resistance and reactance show a maximum around $\Delta\phi = 90°$(Fig. 12(b)). The maximum current drive efficiency is found to be $0.02\ A/W$(Fig. 12(c)) which is much smaller than the low frequency excitation case since the $m = \pm 1$ peaks are accessible and they reduce the current drive efficiency. The antenna current spectrum for $\Delta\phi = 90°$ and $N = 8$ is shown in Fig.13.

The the energy flux, absorption, and induced current profiles are shown in Fig. 14(a) and (b) for $\Delta\phi = 90°$ on the $z = 0$ plane. As the incident fast wave propagates in the central region, power absorption by ions occurs around $x = 0$ and electron absorption occurs in the region, $-0.1\ m < x < 0.1\ m$(Fig. 14(a)). As shown in Fig. 14(b) the induced current profile follows the electron absorption profile. Corrugation in the power absorption and current profile is due to the formation of a standing wave which is clear in the electric field structure shown in Fig. 14(c) and

(d). Due to the high phase velocity of the wave, coupling between the wave and the electrons is weak. The incident wave is not completely absorbed in a single pass and is reflected at the high field side wall. The electrons absorb power in a multi pass process.

5 Summary

We have studied the characteristics of fast wave current drive in a KT-2 tokamak plasma by solving the kinetic equation of the ICRF wave in a one dimensional slab model. To determine the design guidelines for optimum current drive, we investigated the accessibility of the fast wave for low($f = 30\,MHz$) and high($f = 225\,MHz$) frequency cases. From the accessibility conditions, we obtained an optimum launching condition based on the antenna spacing, phase, and total antenna number. For low wave frequency, the accessible k_z region is small and the optimum parallel wave number is found to be $3\,m^{-1}$. For high wave frequency, both $k_{z,min}$ and $k_{z,max}$ increase and the optimum parallel wave number is found to be $18\,m^{-1}$. The wave propagation is dominated by cavity resonance due to the formation of a standing wave in both cases.

For the cases considered in this study, the maximum current drive efficiency is estimated as $0.05\,A/W$ for low frequency excitation with the antenna phase, $\Delta\phi = 70°$ and total antenna number, $N = 8$, although trapped particle effects which usually reduce the current drive efficiency are not considered. Also, a two dimensional treatment in the calculation of electron power absorption, and the calculation of the driven current and its profile which are consistent with the MHD equilibrium are necessary for a more accurate estimation. Many peaks in the power absorption due to cavity resonance are expected to be reduced in the two dimensional analysis. Two dimensional analysis can also include geometrical effects from magnetic surface averaging of the driven current profile. These studies are left for future work.

Acknowledgments

One(B.G. Hong) of the authors would like to thank the JAERI staff for their help during his stay at Japan Atomic Energy Research Institute.

(d). Due to the high phase velocity of the wave, coupling between the wave and the electrons is weak. The incident wave is not completely absorbed in a single pass and is reflected at the high field side wall. The electrons absorb power in a multi pass process.

5 Summary

We have studied the characteristics of fast wave current drive in a KT-2 tokamak plasma by solving the kinetic equation of the ICRF wave in a one dimensional slab model. To determine the design guidelines for optimum current drive, we investigated the accessibility of the fast wave for low($f = 30\,MHz$) and high($f = 225\,MHz$) frequency cases. From the accessibility conditions, we obtained an optimum launching condition based on the antenna spacing, phase, and total antenna number. For low wave frequency, the accessible k_z region is small and the optimum parallel wave number is found to be $3\,m^{-1}$. For high wave frequency, both $k_{z,min}$ and $k_{z,max}$ increase and the optimum parallel wave number is found to be $18\,m^{-1}$. The wave propagation is dominated by cavity resonance due to the formation of a standing wave in both cases.

For the cases considered in this study, the maximum current drive efficiency is estimated as $0.05\,A/W$ for low frequency excitation with the antenna phase, $\Delta\phi = 70°$ and total antenna number, $N = 8$, although trapped particle effects which usually reduce the current drive efficiency are not considered. Also, a two dimensional treatment in the calculation of electron power absorption, and the calculation of the driven current and its profile which are consistent with the MHD equilibrium are necessary for a more accurate estimation. Many peaks in the power absorption due to cavity resonance are expected to be reduced in the two dimensional analysis. Two dimensional analysis can also include geometrical effects from magnetic surface averaging of the driven current profile. These studies are left for future work.

Acknowledgments

One(B.G. Hong) of the authors would like to thank the JAERI staff for their help during his stay at Japan Atomic Energy Research Institute.

(d). Due to the high phase velocity of the wave, coupling between the wave and the electrons is weak. The incident wave is not completely absorbed in a single pass and is reflected at the high field side wall. The electrons absorb power in a multi pass process.

5 Summary

We have studied the characteristics of fast wave current drive in a KT-2 tokamak plasma by solving the kinetic equation of the ICRF wave in a one dimensional slab model. To determine the design guidelines for optimum current drive, we investigated the accessibility of the fast wave for low($f = 30\,MHz$) and high($f = 225\,MHz$) frequency cases. From the accessibility conditions, we obtained an optimum launching condition based on the antenna spacing, phase, and total antenna number. For low wave frequency, the accessible k_z region is small and the optimum parallel wave number is found to be $3\,m^{-1}$. For high wave frequency, both $k_{z,min}$ and $k_{z,max}$ increase and the optimum parallel wave number is found to be $18\,m^{-1}$. The wave propagation is dominated by cavity resonance due to the formation of a standing wave in both cases.

For the cases considered in this study, the maximum current drive efficiency is estimated as $0.05\,A/W$ for low frequency excitation with the antenna phase, $\Delta\phi = 70°$ and total antenna number, $N = 8$, although trapped particle effects which usually reduce the current drive efficiency are not considered. Also, a two dimensional treatment in the calculation of electron power absorption, and the calculation of the driven current and its profile which are consistent with the MHD equilibrium are necessary for a more accurate estimation. Many peaks in the power absorption due to cavity resonance are expected to be reduced in the two dimensional analysis. Two dimensional analysis can also include geometrical effects from magnetic surface averaging of the driven current profile. These studies are left for future work.

Acknowledgments

One(B.G. Hong) of the authors would like to thank the JAERI staff for their help during his stay at Japan Atomic Energy Research Institute.

References

[1] M. Kikuchi and the JT-60 Team, *"Recent JT-60U Results towards Steady State Operation of Tokamaks"*, Plasma Physics and Controlled Nuclear Fusion Research(IAEA, Vienna, 1995) Vol.1, p.31.

[2] P.A. Politzer et al., Phys. Plasmas **1**, p.1545, 1994.

[3] E.A. Lazarus et al., Phys. Fluids B**4**, P.3644, 1992.

[4] E.J. Strait et al., *"Beta-Limiting Instabilities in DIII-D Discharges with Large Bootstrap Current"*, in Proc. 20th Euro. Conf. on Contr. Fusion and Plasma Heating, Lisbon, Portugal, 1993(EPS, Petit-Lancy, Switzerland, 1993).

[5] M. Hugon et al., Nucl. Fusion **32**, p.33, 1992.

[6] G.T. Hoang et al., Nucl. Fusion **34**, p.75, 1994.

[7] T. Kondoh and JT60 Team, Phys. Plasmas **1**, p.1489, 1994.

[8] I.S. Chang et al., *"Concept Definition of KT-2 : a large aspect ratio divertor tokamak with FWCD"*, KAERI/TR-472/94, 1994.

[9] S.C. Chiu et al., Nuclear Fusion **29**, p.2175, 1989.

[10] N.J. Fisch and C.F.F. Karney, Phys. Fluids **24**, p.27, 1981.

[11] C.N. Lashmore-Davies et al., Phys. Fluids **31**, p.1614, 1988.

[12] Y. Kishimoto et al, Nucl. Fusion **27**, p.549, 1987.

[13] A. Fukuyama et al., Nucl. Fusion **23**, p.1005, 1983.

[14] K. Hamamatsu et al, Nucl. Fusion **29**, p.147, 1989.

[15] B.D. McVey, Nucl. Fusion **19**, p.461, 1979.

[16] D.A. Ehst and C.F.F. Karney, Nucl. Fusion **31**, p.1933, 1991.

[17] K. Hamamatsu et al., Jpn. J. Appl. Phys. **26**, p.1525, 1987.

Table 1 Reference parameters of KT－2 Tokamak

major radius	R_0	1.4 m
minor radius	a	0.25 m
antenna radius	d	0.27 m
wall radius	b	0.35 m
toroidal field	B_0	3.0 T
density	n_0	$1.0\times10^{20}m^{-3}$
temperature	$T_{e0} = T_{H0}$ $T_{eb} = T_{Hb}$	5 keV 0.01 keV
frequency	f	30 *MHz* 225 *MHz*
effective charge	Z_{eff}	2.0

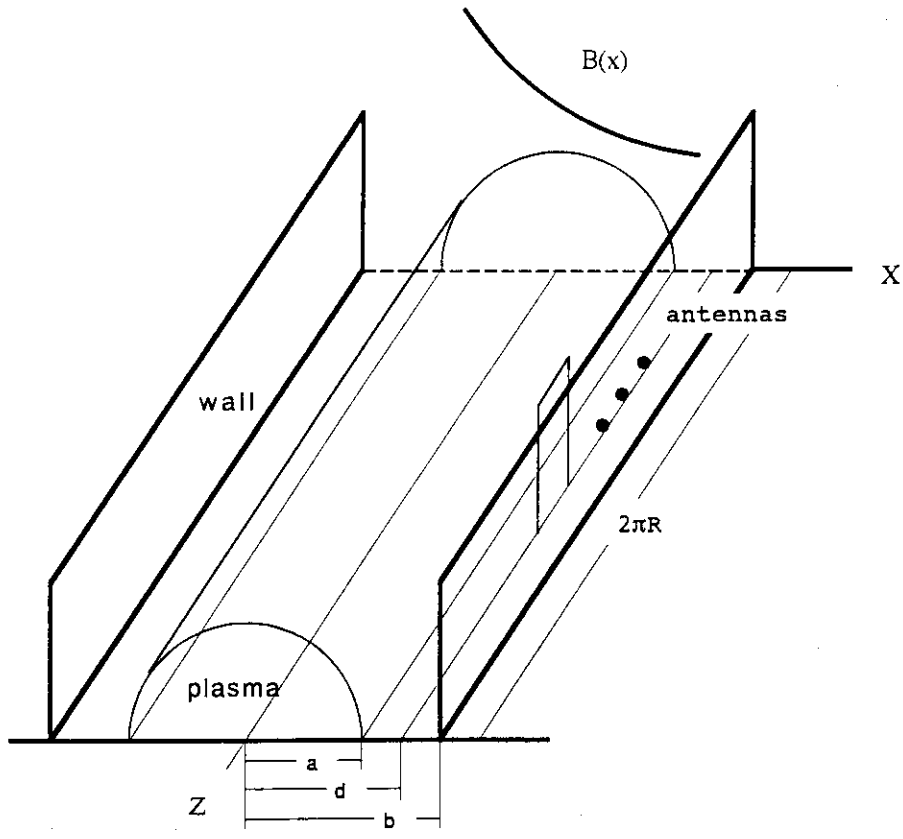

Fig. 1 Model configuration of ICRF wave propagation. Multi-antennas are positioned at low field side (x =d), Standard parameters are given in Table 1.

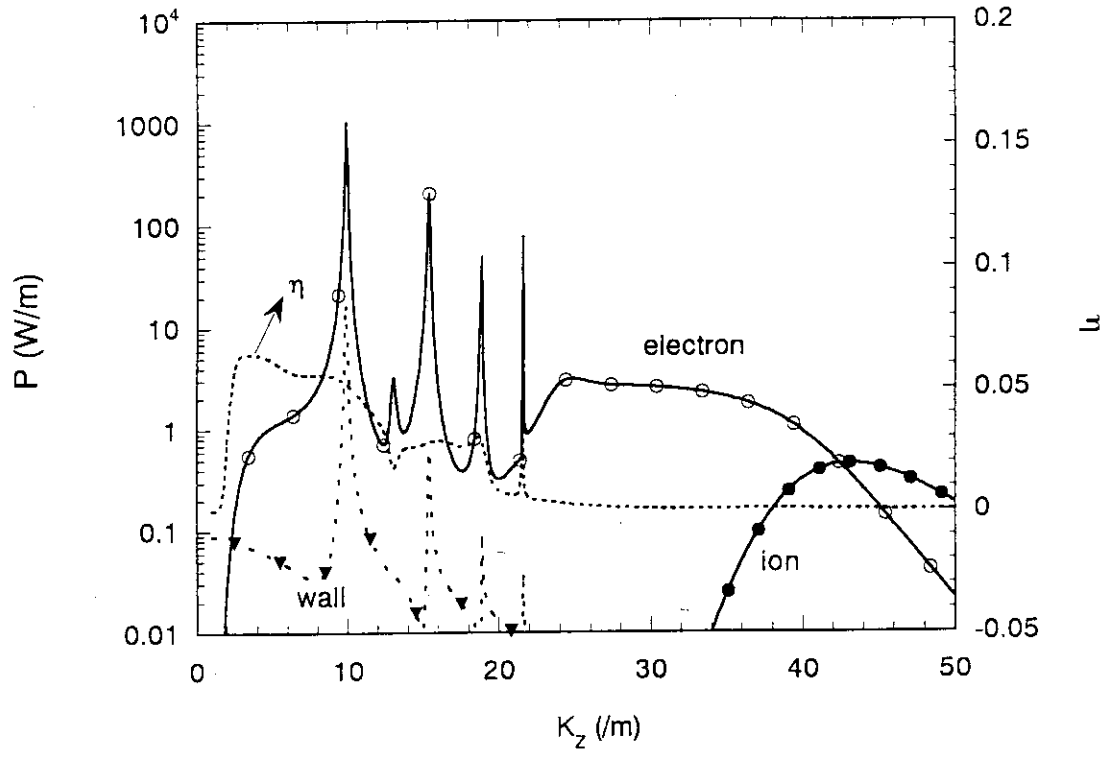

Fig. 2 Absorption power spectrum, $\overline{P}_s$ as a function of k_z for $n_0 = 1 \times 10^{20}\,m^{-3}$, $T_0 = 5\,keV$ and $f = 30\,MHz$.

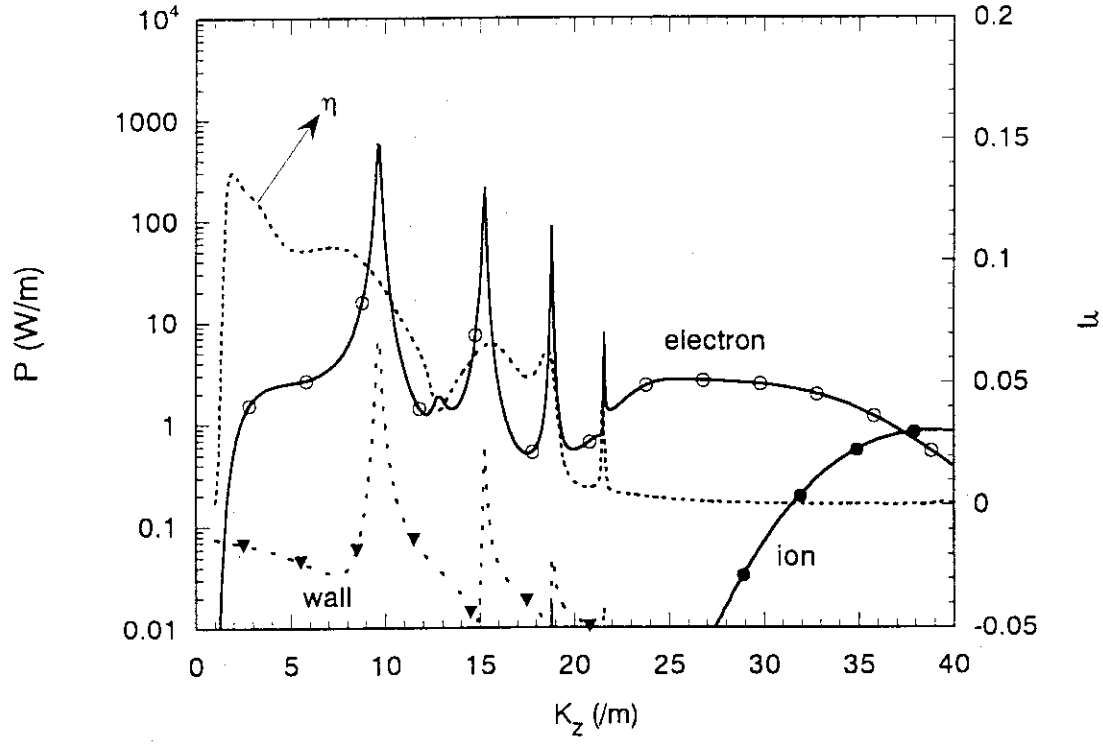

Fig. 3 Absorption power spectrum, $\overline{P}_s$ as a function of k_z for $n_0 = 1 \times 10^{20}\,m^{-3}$, $T_0 = 10\,keV$ and $f = 30\,MHz$.

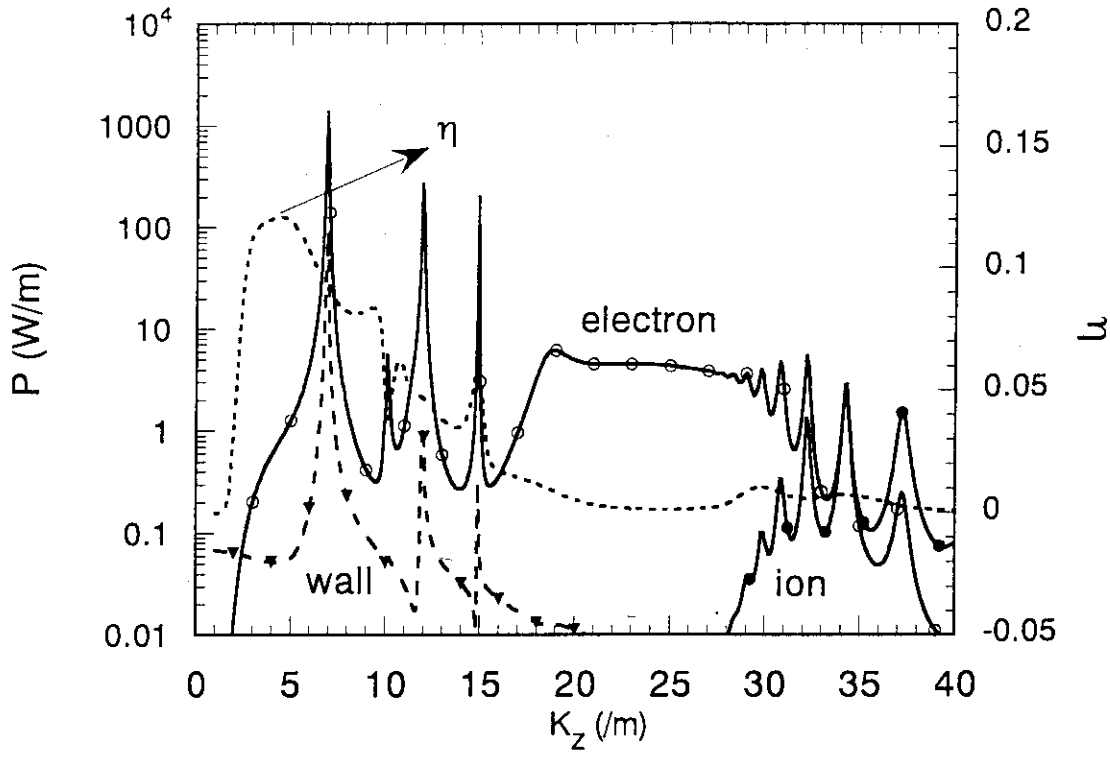

Fig. 4 Absorption power spectrum, $\overline{P}_s$ as a function of k_z for $n_0 = 0.5 \times 10^{20}\,m^{-3}$, $T_0 = 5\,keV$ and $f = 30\,MHz$.

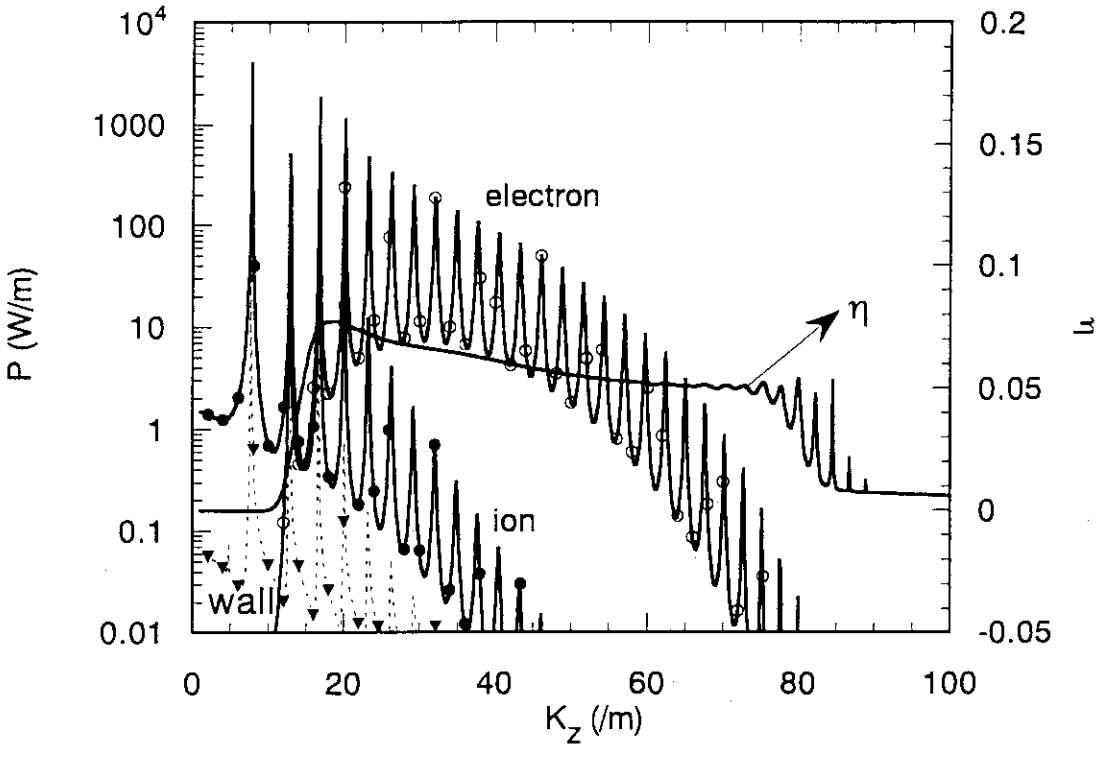

Fig. 5 Absorption power spectrum, $\overline{P}_s$ as a function of k_z for $n_0 = 1 \times 10^{20}\,m^{-3}$, $T_0 = 5\,keV$ and $f = 225\,MHz$.

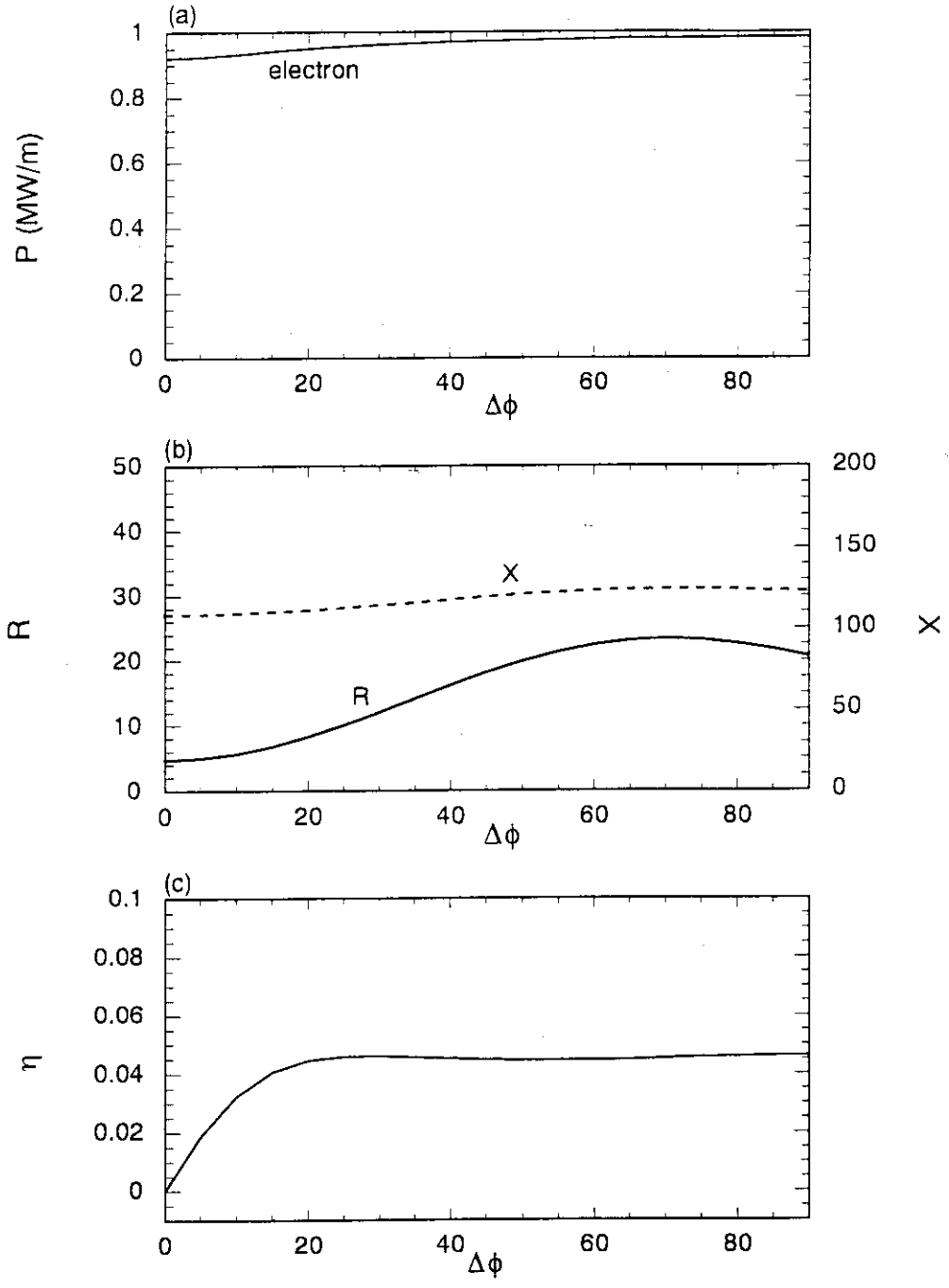

Fig. 6 Phase dependence of (a) power absorbed by electrons, (b) average loading resistance (Ω／m) and reactance (Ω／m) per antenna, and (c) current drive efficiency (A／W) for the case of $N = 4$ and $\Delta z = 12.2$ cm.

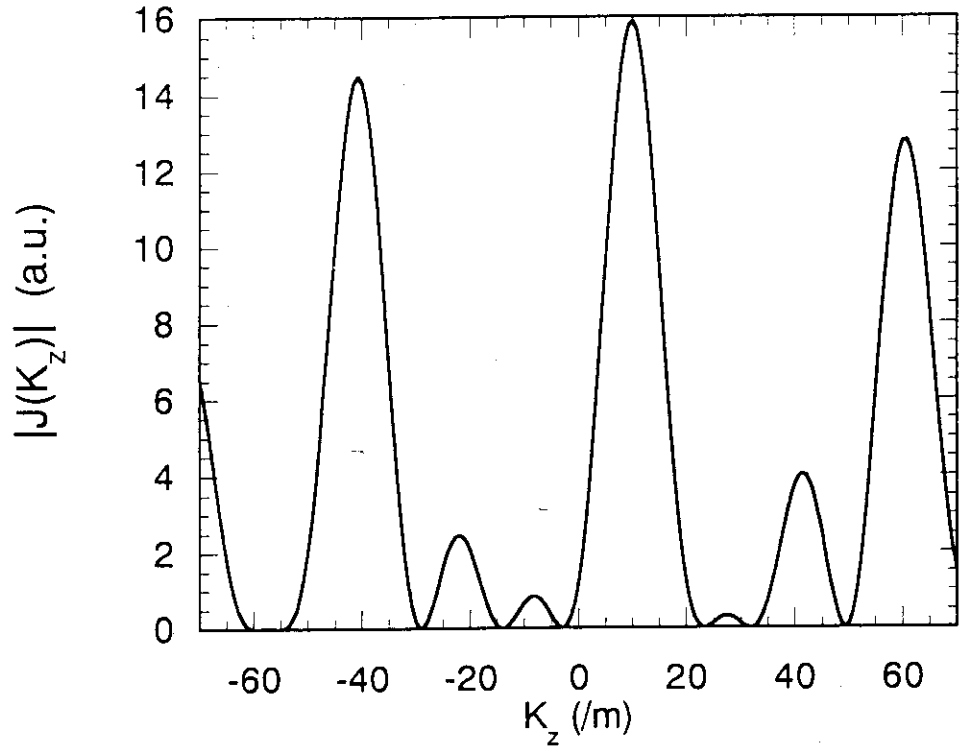

Fig. 7 Spectrum of antenna current for N = 4 and $\Delta\phi = 70°$.

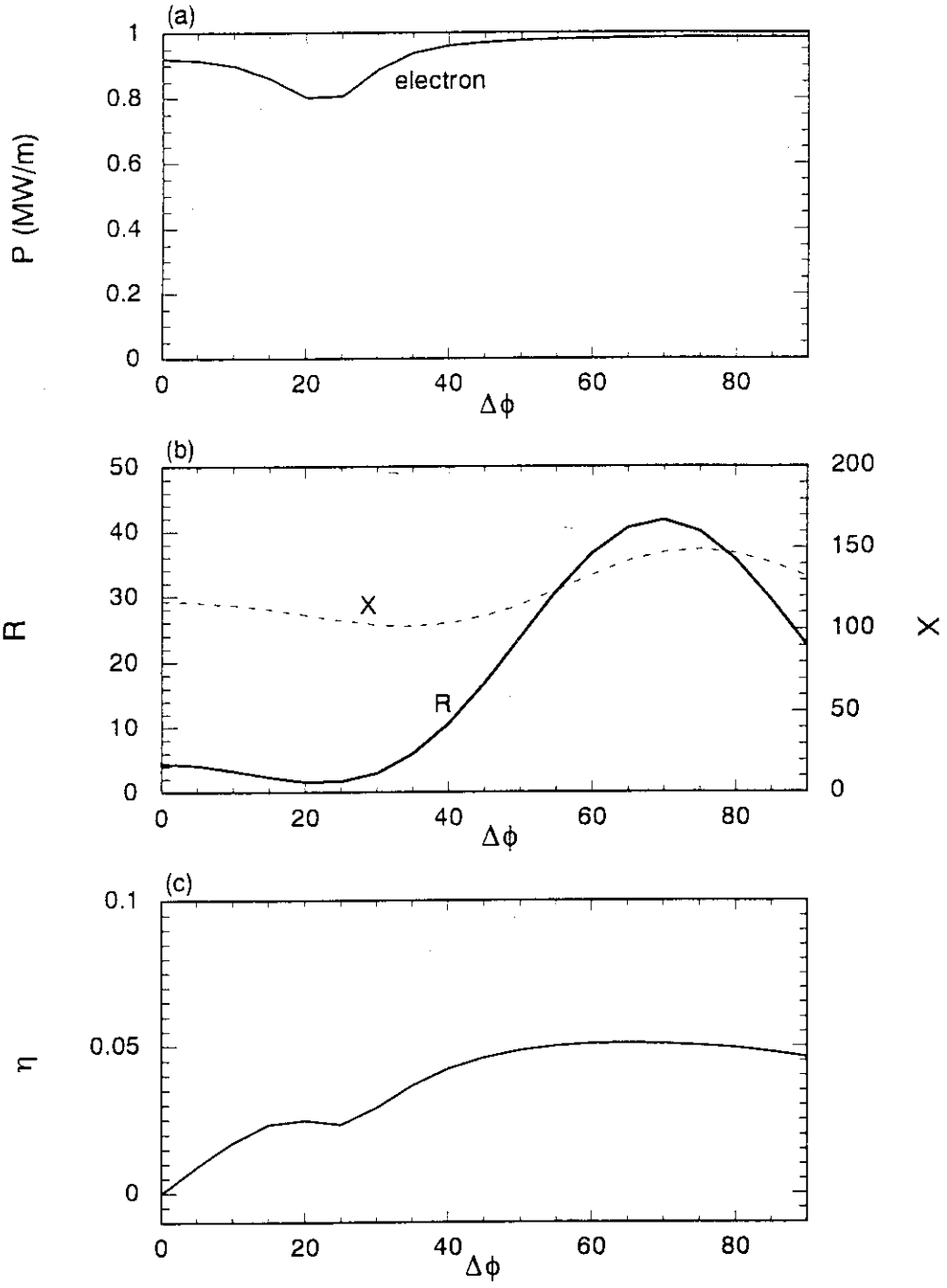

Fig. 8 Phase dependence of (a) power absorbed by electrons, (b) average loading resistance (Ω／m) and reactance (Ω／m) per antenna, and (c) current drive efficiency (A／W) for the case of N＝8 and Δz＝12.2 ㎝.

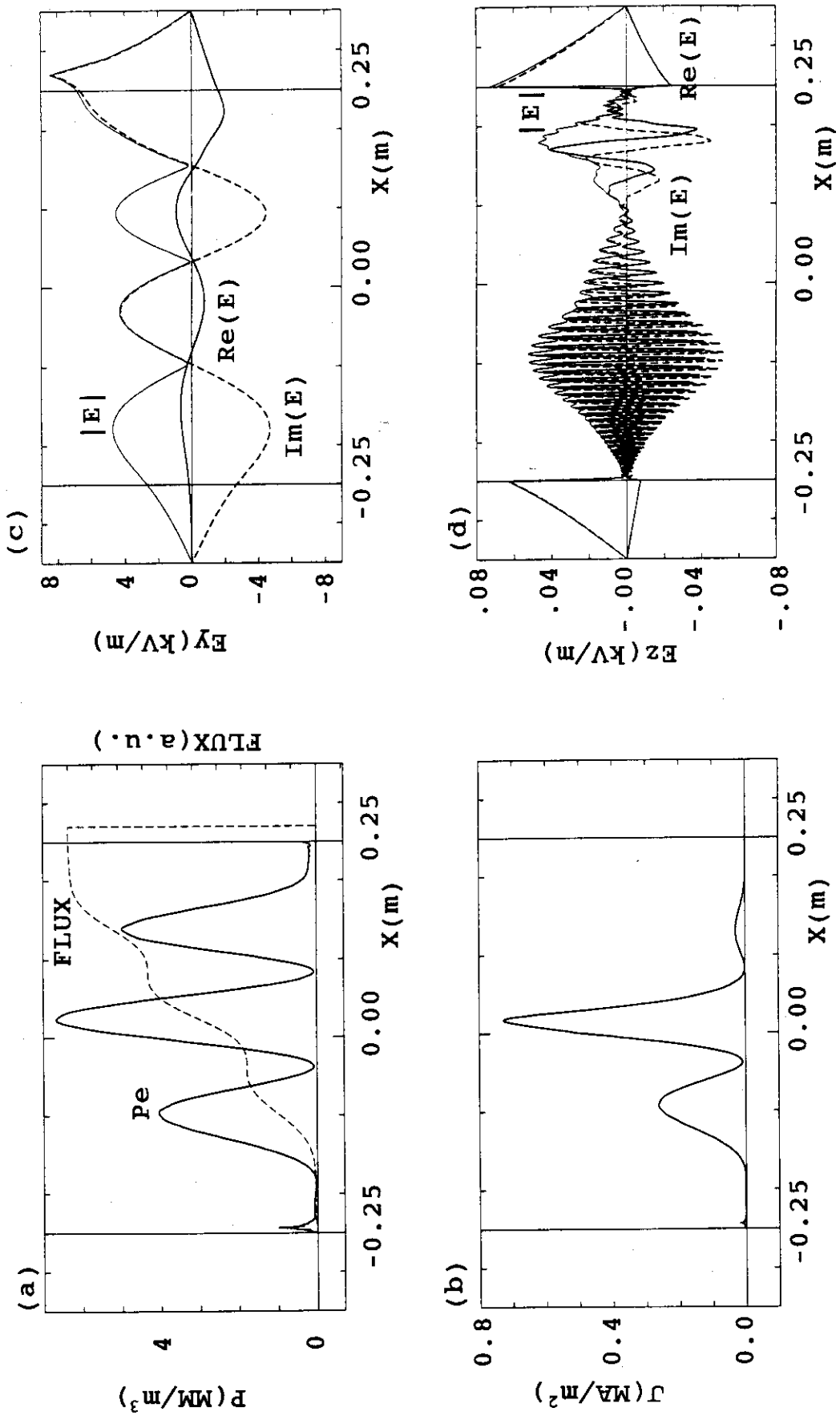

Fig. 9 Spatial structure of (a) energy flux and power absorbed by electrons, (b) induced current, and electric fields, (c) E_y and (d) E_z in the $z = 0$ plane for the case of $N = 8$ and $\Delta\phi = 70°$.

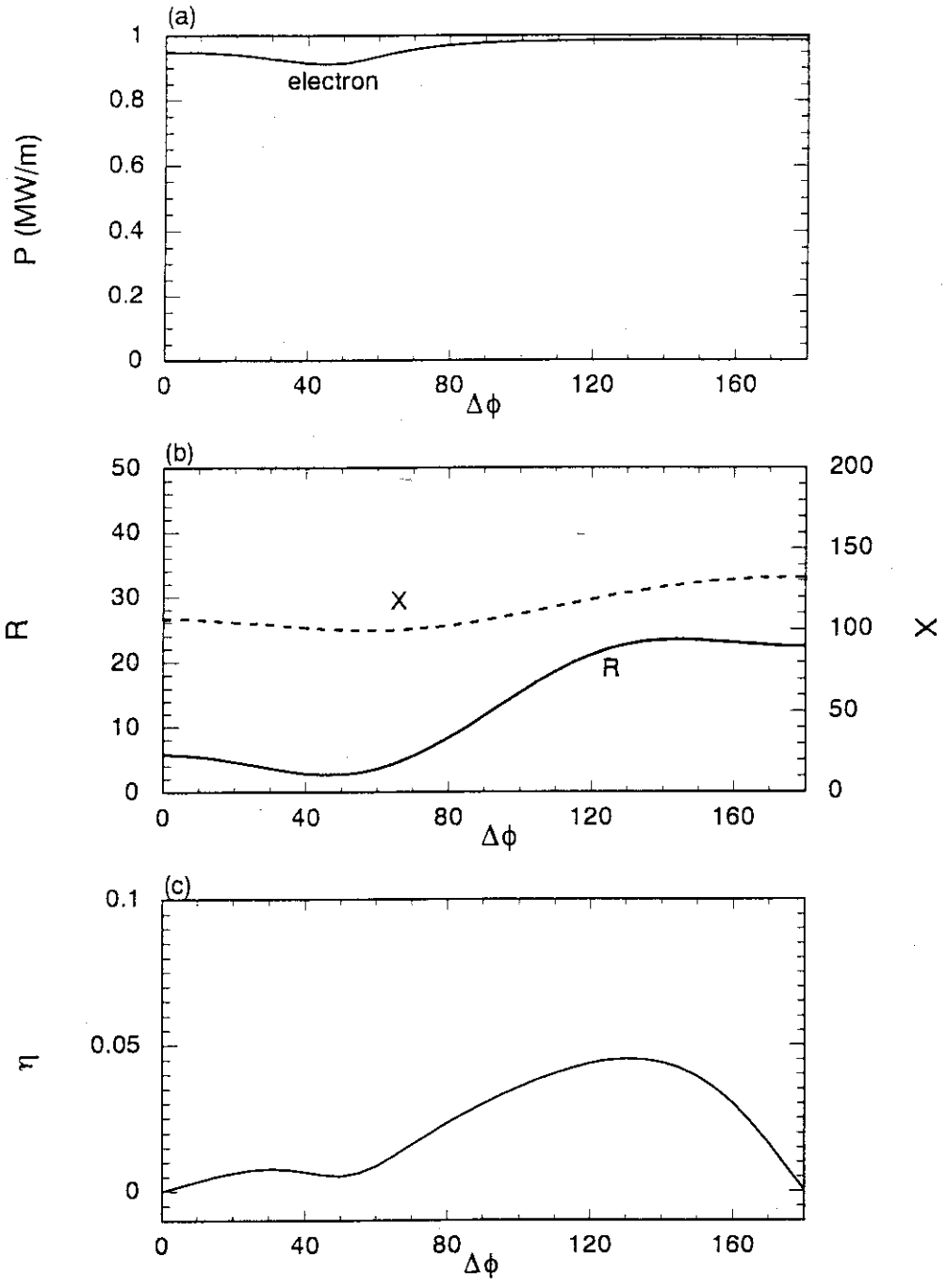

Fig. 10 Phase dependence of (a) power absorbed by electrons, (b) average loading resistance (Ω／m) and reactance (Ω／m) per antenna, and (c) current drive efficiency (A／W) for the case of N = 4 and Δz = 24.4 cm.

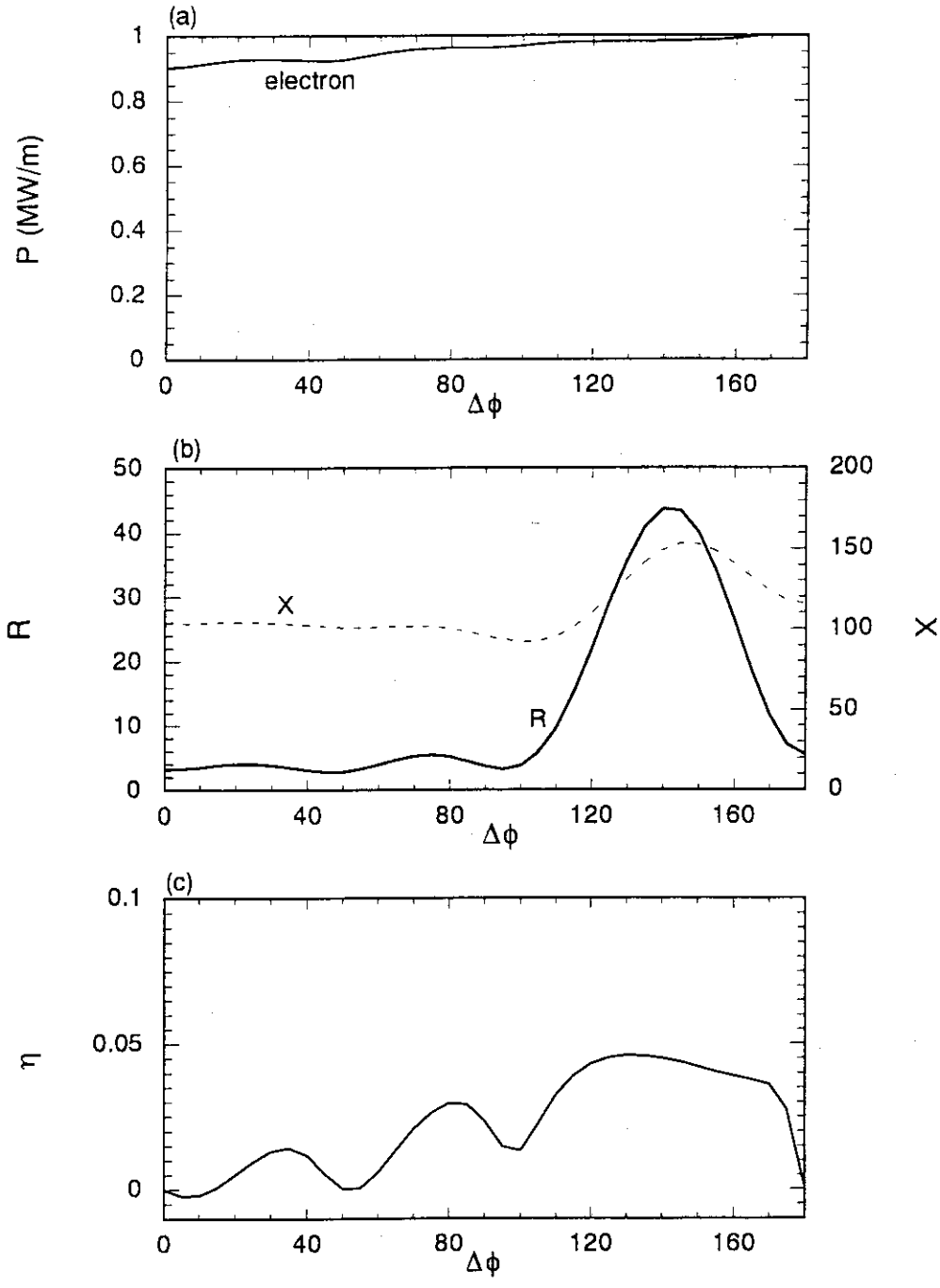

Fig. 11 Phase dependence of (a) power absorbed by electrons, (b) average loading resistance (Ω／m) and reactance (Ω／m) per antenna, and (c) current drive efficiency (A／W) for the case of N = 8 and Δz = 24.4 cm.

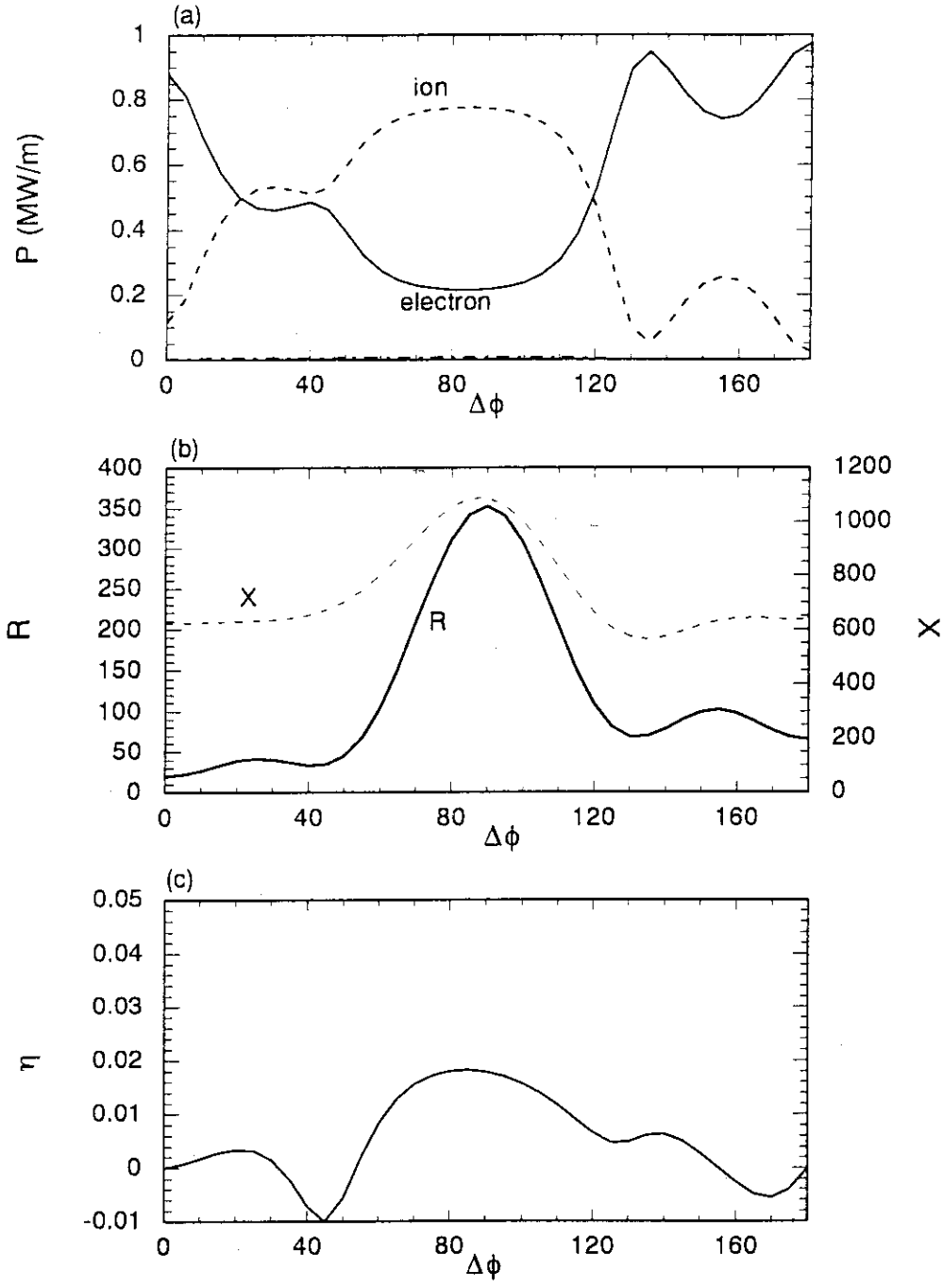

Fig. 12 Phase dependence of (a) power absorbed by electrons, (b) average loading resistance (Ω／m) and reactance (Ω／m) per antenna, and (c) current drive efficiency (A／W) for the case of N = 8, Δz = 12.2 cm and f = 225 MHz.

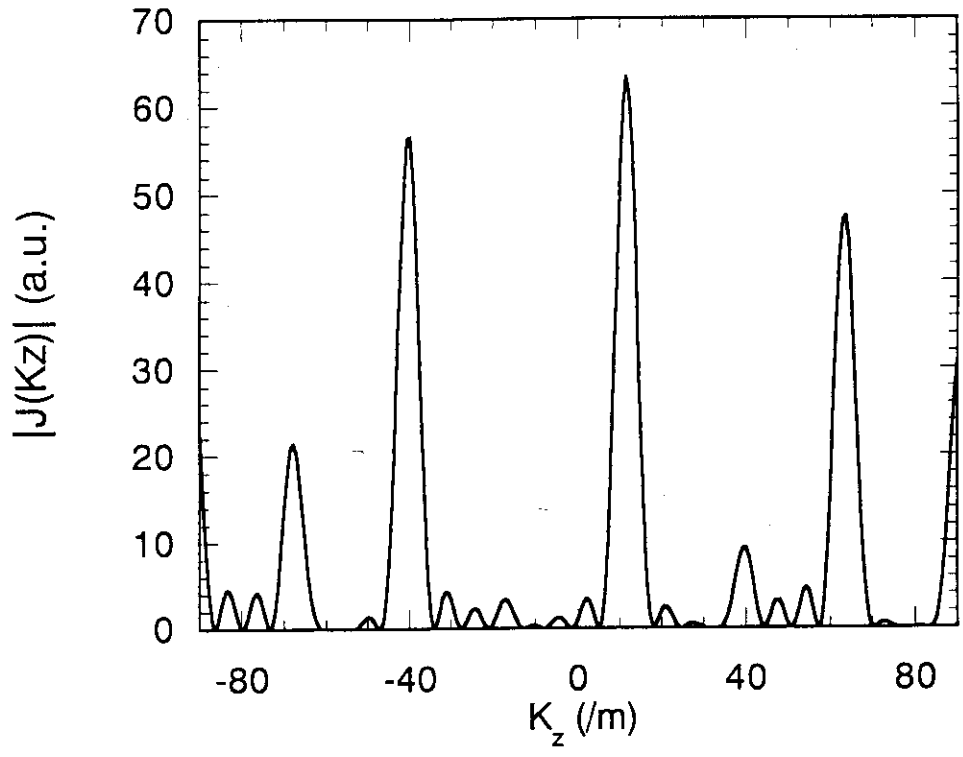

Fig. 13 Spectrum of antenna current for N = 8 and $\Delta\phi = 90°$.

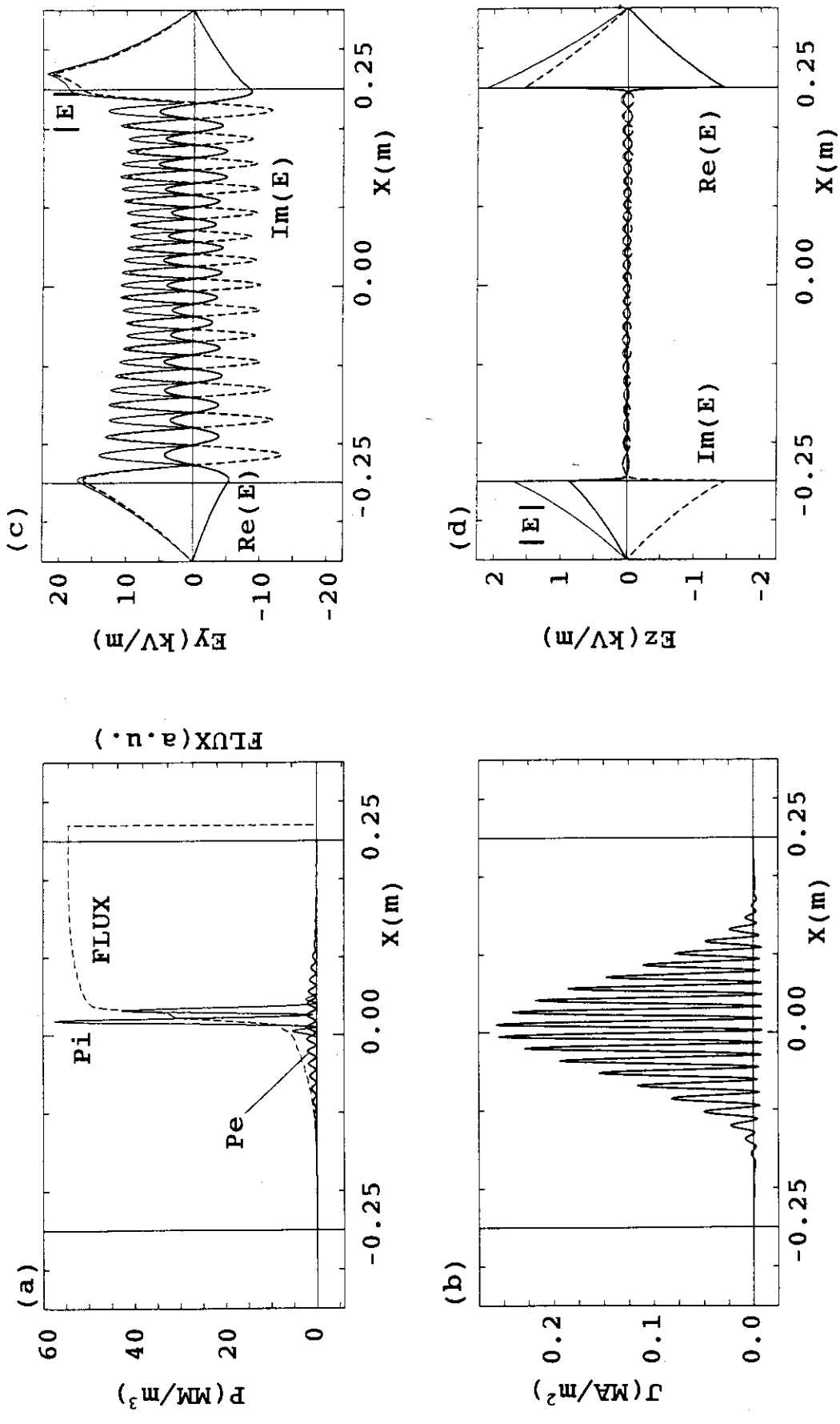

Fig. 14 Spatial structure of (a) energy flux and power absorbed by electrons, (b) induced current, and electric fields, (c) E_y and (d) E_z in the $z = 0$ plane for the case of $N = 8$, $\Delta\phi = 90°$ and $f = 225$ MHz.